Hyperspectral signal reconstruction from interferometric measurements with enriched Fourier bases

Yassine Mhiri, Rémy Abergel, Andrés Almansa, Lionel Moisan
Université Paris Cité, CNRS, MAP5, F-75006 Paris, France

***Abstract*—Fourier Transform Spectrometers are instruments that measure the spectral distribution of an electromagnetic signal. They are based on the principle of interferometry, which leverages interference patterns to reconstruct high-resolution observations by solving an inverse problem defined on a continuous domain. The forward model is a linear integral operator, which is, in most cases, discretized by considering a uniform grid and associated Riemann sums to estimate integrals. This approximation introduces an important reconstruction error, which can be significantly reduced by using instead appropriate bases of functions to represent the signal of interest. In this paper, we show the judiciousness of the Fourier basis for this problem, and highlight through numerical experiments the gain it brings in terms of reconstruction precision, compared to the classical use of discrete samples. We finally propose a new basis obtained by enriching the Fourier basis with an affine component, which allows us to overcome the inherent difficulty of representing non-periodic functions with a finite number of sine functions. We show that this new basis leads to another significant improvement of the reconstruction error.**

***Index Terms*—Fourier Transform Spectrometers, Interferometry, Linear integral operators, Hyperspectral imaging, Inverse problems**

I. Introduction

Spectrometers are used in many scientific and industrial fields, such as chemistry, physics, biology, and medicine. In particular, spectrometers embedded on satellites make it possible to obtain measurements of the reflectance of the earth's surface in the visible and near-infrared spectrum, from which key informations can be extracted about the vegetation, pollution, and topography. They provide essential information for understanding the evolution of the earth's surface and its climate.

A wide variety of spectrometers have been developed in recent decades. Among them, Fourier Transform Spectrometers (FTS) have improved the performance of traditional instruments in terms of spectral resolution and sensitivity by designing new acquisition systems by interferometry [1], [2]. These instruments measure samples of the Fourier transform of the incident spectrum and then proceed to a discrete inverse Fourier transform for reconstruction. For this, an interferometric system is designed in which phase-shifted versions of the incident wave interfere, producing a so-called interference signal. This signal is related to the Fourier transform of the incident spectrum at a frequency given by the optical path difference (OPD) between the phase-shifted versions of the wave. Thus, the choice of the OPDs is crucial in the design of such an instrument, as it determines the spectral range it can cover and the spectral resolution it can achieve. Different applications may then require different designs. For example, the detection of atmospheric gases requires a very fine spectral resolution around the absorption wavelengths of the gases [3]. On the contrary, detecting vegetation requires measuring the spectrum over a broader range of wavelengths [4]. Due to their compactness and low cost, FTS are integrated into several ongoing and future space missions aiming at better measuring the anthropogenic emissions of greenhouse gases [1], [2].

The spectrum reconstruction from the measurements is then carried out by solving an inverse problem. To do so, a precise knowledge of the forward model is necessary. In particular, in interferometric spectrometers, the forward model is a linear integral operator, and the inverse problem is defined in a continuous domain. A discretization of the forward operator is required to solve the inverse problem numerically. This discretization is often carried out explicitly by considering a uniform grid from which a Riemann sum is built to approximate the integral [5]. However, this approximation introduces an error in the reconstruction and might result in highly computationally demanding algorithms.

Recent works have shown an interest in considering more sophisticated discretizations of the integral operator in the context of image deblurring [6]. They consider an approximation of the signal of interest in a judiciously chosen basis of functions. Notably, wavelet bases have been considered to approximate blur operators and have shown promising results in terms of computational complexity, memory footprint, and reconstruction precision [6], [7]. Some of these approaches are based on the Galerkin method, initially used to approximate linear integral operators in the study of pseudo-differential equations [8].

Such methodology has yet to be studied in the context of signal reconstruction from interferometric measurements. This offers an excellent potential for the design of reconstruction algorithms in terms of computational efficiency and reconstruction precision. In this paper, we study the interest of Fourier-based function bases to discretize the integral operator involved in an FTS. In sections II and III, we present the linear integral operator associated to the forward model of a FTS, and we formulate the inverse problem to be solved in a continuous domain. In Section IV, two function bases are

considered and studied: the Fourier basis, and a new basis enriched with an affine component so as to avoid Gibbs effects (and poor approximation performances) in the reconstruction of signals that do not vanish at both ends of the spectral range. Finally, we illustrate the interest of the proposed approaches on simulated data through numerical experiments.

II. Fourier Transform Spectrometers

FTS sample a transformation y of the incident light spectrum x by producing fringes using an interfering device, where

$$y(\delta) = \langle \mathcal{A}(\delta, \cdot), x \rangle := \int_{\sigma_{\min}}^{\sigma_{\max}} \mathcal{A}(\delta, \sigma) x(\sigma) \mathrm{d}\sigma, \qquad (1)$$

$\delta > 0$ is the optical path difference (OPD) between the phase-shifted versions of the incident wave introduced by the interfering device, and the transfer function $\mathcal{A}(\delta, \sigma)$ is derived through the physical system that produces the interfering fringes. The input spectrum, $x \in \mathcal{X} = L^2([\sigma_{\min}, \sigma_{\max}])$, is a function of the wavenumber σ (measured in μm^{-1}) and corresponds to its continuous representation in the wavenumber range $[\sigma_{\min}, \sigma_{\max}]$ to which the instrument is sensitive. An FTS measures the interference signal for a set of OPD values $\delta_0, \ldots, \delta_{M-1}$, leading to a measurement vector of dimension M, written

$$\boldsymbol{y} = (y(\delta_0), \ldots, y(\delta_{M-1}))^T. \qquad (2)$$

The transfer function of an FTS is usually expressed using trigonometric functions. In the following, we consider the case of the ImSPOC instrument, a hyperspectral imager based on a network of adjacent Fabry-Pérot interferometers [9], for which

$$\mathcal{A}(\delta, \sigma) = (1 - R)^2 \left| \sum_{n=0}^{+\infty} R^n e^{\mathrm{j}\, 2\pi n \delta \sigma} \right|, \qquad (3)$$

in which $0 < R < 1$ is the reflectivity of the interferometers. The incoming wave is phase-shifted and attenuated by successive reflections before interfering with its other replicas in the sensor. This ideal model expresses the interference between an infinite number of waves. However, in practice, the value of R will cause a fast decay of the power of the reflected waves. Thus, practical models of the transfer function consider a finite number of interfering waves, depending on the reflectivity value. In [9], it is shown that a 2-waves model is appropriate to express the measured data for $R \leq 0.3$, leading to,

$$\mathcal{A}^{[2]}(\delta, \sigma) = (1 - R)^2 \left(1 + R^2 + 2R \cos(2\pi\delta\sigma)\right). \qquad (4)$$

The 2-waves model can be interpreted using the cosine transform of the input spectra, since for $\mathcal{A} = \mathcal{A}^{[2]}$, (1) becomes

$$y(\delta) = (1 - R)^2 \Big((1 + R^2)\overline{x} + 2R\ \Re\{\mathcal{F}\{x\}(\delta)\} \Big) \qquad (5)$$

where $\overline{x} = \int_{\sigma_{\min}}^{\sigma_{\max}} x(\sigma)\, \mathrm{d}\sigma$, $\mathcal{F}\{x\}$ is the Fourier Transform of x and $\Re\{z\}$ denotes the real part of a complex number $z \in \mathbb{C}$. Thus, ImSPOC measurements can be interpreted as samples of the cosine transform of the input spectra. In particular, the maximum OPD value of the instrument, $\delta_{\max}$, determines the theoretical spectral resolution achievable by the instrument, $\frac{1}{2\delta_{\max}}\ \mu m$, thanks to Shannon-Nyquist Sampling Theorem. Without loss of generality, we will consider in the following the 2-waves model. Indeed, similarly to the 2-waves model, the N-waves model can be expressed as the sum of cosine transforms (as shown in [9]).

III. Inverse problem formulation

We can observe that the set of measurements provided by an FTS instrument are described by the composition of two operators: a linear integral operator with kernel $\mathcal{A}$ (Equation (1)), and a sampling operator (Equation (2)). Given the measurements $\boldsymbol{y}$, the reconstruction of the spectrum x can be addressed as a variational inverse problem. The most common approach corresponds to the least squares energy minimization,

$$\widehat{x} \in \operatorname*{argmin}_{x \in \mathcal{X}} \sum_{m=0}^{M-1} \big(y(\delta_m) - \langle \mathcal{A}(\delta_m, \cdot), x \rangle \big)^2. \qquad (6)$$

As this inverse problem is defined in a continuous domain, it cannot be solved numerically as it is, but it has to be first reduced to a finite-dimensional problem. A natural way to discretize (6) is to sample the unknown function $x(\sigma)$ on the regular grid $(\sigma_k)_{0 \leq k \leq K-1}$ defined by

$$\sigma_k = \sigma_{\min} + k \frac{\Delta_\sigma}{K} \quad \text{and} \quad \Delta_\sigma = \sigma_{\max} - \sigma_{\min},$$

leading to the discrete signal

$$\boldsymbol{x} = (x(\sigma_0), \ldots, x(\sigma_{K-1}))^T. \qquad (7)$$

The integral in (1) is then approximated by a Riemann sum, leading to the discrete model

$$y(\delta_m) = \frac{\Delta_\sigma}{K} \sum_{k=0}^{K-1} \mathcal{A}(\delta_m, \sigma_k)\, x(\sigma_k) = \boldsymbol{a}_m^T \boldsymbol{x}, \qquad (8)$$

$$\text{where} \quad \boldsymbol{a}_m = \frac{\Delta_\sigma}{K} (\mathcal{A}(\delta_m, \sigma_0), \ldots, \mathcal{A}(\delta_m, \sigma_{K-1}))^T.$$

A simple and compact reformulation of this discretization model is given by the matrix equation

$$\boldsymbol{y} = \boldsymbol{A}\boldsymbol{x} \qquad (9)$$

with $\boldsymbol{A} = (\boldsymbol{a}_0, \ldots, \boldsymbol{a}_{M-1})$.

Despite the simplicity of this discretization scheme, important reconstruction errors may occur when the sampling grid is not fine enough, due to the poor approximation of the continuous integral provided by the Riemann sum. It is thus desirable to choose a large value of K, but when $K > M$ the inversion of (9) becomes an ill-posed problem (the number of unknowns is greater than the number of available measurements), so that a regularizing term has to be added to the model, which leads to a more complex algorithm and a higher computational cost. In response, a few approaches have been proposed to tackle the discretization of linear integral operators in an inverse problem setting. In particular, a methodology based on the wavelet representation of the kernel has been

considered in the context of image deblurring and has shown promising results [6], [7]. In the following we shall propose another discretization scheme for (1), relying on Fourier-based decompositions of the spectrum to be reconstructed.

IV. Using Fourier-based approximations

Let $(f_0, \dots, f_{K-1})$ be a set of basis functions and let us consider $\mathcal{X}_K = \operatorname{span}(f_0, \dots, f_{K-1})$ as an approximation space containing all candidate spectra for the reconstruction. Thus, any candidate spectrum $x \in \mathcal{X}_K$ can be written under the form

$$\forall \sigma \in \Omega, \quad x(\sigma) = \sum_{k=0}^{K-1} c_k f_k(\sigma), \tag{10}$$

where $(c_0, \dots, c_{K-1}) \in \mathbb{K}^K$ (with $\mathbb{K} = \mathbb{R}$ or $\mathbb{C}$) are real or complex coefficients (depending on the nature of the basis functions). Injecting Equation (10) into (1), we get

$$y(\delta) = \sum_{k=0}^{K-1} c_k \langle \mathcal{A}(\delta, \cdot), f_k \rangle, \tag{11}$$

which can be evaluated for all $\delta \in \{\delta_0, \dots, \delta_{K-1}\}$ to yield another discrete model with matricial structure,

$$\boldsymbol{y} = \boldsymbol{H}\boldsymbol{c}, \tag{12}$$

in which $\boldsymbol{c} = (c_0, \dots, c_{M-1})^T$ and $\boldsymbol{H}$ is the $M \times K$ matrix with entries $\boldsymbol{H}_{m,k} = \langle \mathcal{A}(\delta_m, \cdot), f_k \rangle$. Thus, restricting the candidate spectra x in the continuous least squares problem (6) to lie into the approximation space $\mathcal{X}_K$, we end up with the finite-dimensional problem of computing

$$\widehat{x} = \sum_{k=0}^{K-1} \widehat{c}_k f_k \quad \text{where} \quad \widehat{\boldsymbol{c}} \in \operatorname*{argmin}_{\boldsymbol{c} \in \mathbb{K}^K} \|\boldsymbol{y} - \boldsymbol{H}\boldsymbol{c}\|^2. \tag{13}$$

Note that the choice of the basis functions is crucial since it acts as a regularization of the inverse problem. In fact, given a ground-truth spectrum, $x^* \in \mathcal{X}$, the best achievable reconstruction in the approximation space is given by its orthogonal projection in $\mathcal{X}_K$,

$$x_K^* = \operatorname{proj}_{\mathcal{X}_K}(x) = \operatorname*{argmin}_{x \in \mathcal{X}_K} \|x - x^*\|^2, \tag{14}$$

since for any $x \in \mathcal{X}_K$,

$$\|x^* - x\|^2 = \|x^* - x_K^*\|^2 + \|x_K^* - x\|^2 \geq \|x^* - x_K^*\|^2. \tag{15}$$

We can recognize in (15) the classical bias-variance decomposition of the squared reconstruction error : the first term $\|x^* - x_K^*\|^2$ is the inevitable component of the error due to the use of an approximation space $\mathcal{X}_K$, and the second term $\|x_K^* - x\|^2$ is the variable part of the reconstruction error due to the presence of noise in the observed measurements.

A. Fourier basis functions

Fourier bases come as natural choices to define the approximation space in the context of interferometric image reconstruction. In fact, the family $\{e^{\mathrm{j}\, 2\pi \frac{k\sigma}{\Delta_\sigma}}\}_{k \in \mathbb{Z}}$ is an orthonormal basis of $\mathcal{X}$. Thus, the signal of interest can be expressed by its Fourier series,

$$x(\sigma) = \sum_{k \in \mathbb{Z}} \alpha_k e^{\mathrm{j}\, 2\pi \frac{k\sigma}{\Delta_\sigma}}, \tag{16}$$

in which $\alpha_k = \langle x, \sigma \mapsto e^{\mathrm{j}\, 2\pi \frac{k\sigma}{\Delta_\sigma}} \rangle$ are the Fourier coefficients of x. Subsequently, we define the set of basis functions $(f_0, \dots, f_{K-1})$ for K odd and $k \in \{0, 1, \dots, K-1\}$ by

$$f_k(\sigma) = \exp\left(\frac{\mathrm{j}\, 2\pi\sigma}{\Delta_\sigma}\left(k - \frac{K-1}{2}\right)\right). \tag{17}$$

The orthogonal projection of x on $\mathcal{X}_K$ is obtain by truncation of the Fourier series (16). More precisely, we have

$$x_K(\sigma) = \sum_{k=-\frac{K-1}{2}}^{\frac{K-1}{2}} \alpha_k e^{\mathrm{j}\, 2\pi \frac{k\sigma}{\Delta_\sigma}} = \sum_{k=0}^{K-1} \alpha_{k-\frac{K-1}{2}} f_k(\sigma). \tag{18}$$

The approximation error between x and its projection x_K on $\mathcal{X}_K$ is controlled by the decay of the Fourier coefficients $(\alpha_k)_{k \in \mathbb{Z}}$ of x. In particular, Fourier coefficients of smooth signals decay as a power law, $\alpha_k = O(|k|^{-\gamma})$, with $\gamma > 0$, giving a bound on the approximation error [10, Chapter 9].

Under this framework, the forward model can then be discretized by computing the entries of the matrix $\boldsymbol{H}$ involved in the discrete model (12). In particular, the natural link between the expression of the linear integral operator for interferometric instruments and the Fourier transform enables the computation of those entries in closed form. Indeed, for the ImSPOC instrument, they are given by

$$\begin{aligned}\langle \mathcal{A}(\delta_m, \cdot), f_k \rangle =& (1-R)^2 \Bigg((1+R^2)\Psi\left(\frac{k}{\Delta_\sigma}\right) + \\ & R\left(\Psi\left(\frac{k}{\Delta_\sigma} + \delta_m\right) + \Psi\left(\frac{k}{\Delta_\sigma} - \delta_m\right)\right)\Bigg),\end{aligned} \tag{19}$$

$$\text{where} \quad \Psi(\nu) = \Delta_\sigma e^{-\mathrm{j}\, \pi(\sigma_{\max}+\sigma_{\min})\nu} \operatorname{sinc}(\pi\nu\Delta_\sigma), \tag{20}$$

and $\operatorname{sinc}(t) = \frac{\sin(t)}{t}$ (with the convention $\operatorname{sinc}(0) = 0$).

Notice that wavelet bases could also have been considered as a relevant alternative to the Fourier basis presented above. Indeed, wavelet bases are known for their universal approximation properties and exhibit, in some cases, faster decay of their coefficients. However, contrary to the Fourier basis which here enables a straightforward computation of the entries of $\boldsymbol{H}$ using (19), the choice of a wavelet basis would in general involve the computation of inner products $\langle \mathcal{A}(\delta_m, \cdot), f_k \rangle$ with non closed form, and would thus come with a higher computational cost [6].

B. Fourier basis enriched with an affine function

We now consider the possibility of enriching the Fourier basis proposed above with functions that constitute a dictionary to represent the spectrum of interest. In this section, we study the possibility of completing the Fourier basis with an affine function, and define for $0 \leq k \leq K-1$ (with K even)

$$f_k(\sigma) = \begin{cases} \exp\left(-\frac{\mathrm{j}\,2\pi\sigma}{\Delta_\sigma}\left(k - \frac{K-2}{2}\right)\right), & \text{if } k \leq K-2 \\ \sigma & \text{if } k = K-1. \end{cases} \quad (21)$$

Contrary to the Fourier basis above, this enriched basis permits the representation of continuous signals $x(\sigma)$ that do not satisfy the constraint $x(\sigma_{\min}) = x(\sigma_{\max})$. The discretization of the integral operator in this case is similar to that proposed for Fourier bases. In fact, this modeling allows an explicit calculation of the inner products between the kernel of the operator and the basis functions by leveraging the properties of the Fourier transform.

V. Numerical experiments

A. Experimental setup

This section presents numerical experiments to illustrate the interest of the proposed approach. We consider an ImSPOC instrument with $M = 319$ interferometers and a wavenumber range $[\sigma_{\min}, \sigma_{\max}] = [0.35, 2.875]\ \mu m^{-1}$. The reflectivity of the interferometers is set to $R = 0.3$ and is assumed to be constant for all interferometers across the wavenumber range. The interferometer thicknesses are chosen so as to obtain a regular sampling of the OPD domain, $\delta_m = \frac{m}{M}\delta_{\max}$, with $\delta_{\max} = 55\mu m$. The measurement data are simulated from a high-resolution spectrum ($N = 2151$ samples) originating from the ECOSTRESS Spectral Library [11]. To do so, we consider the continuous spectrum $x^*(\sigma)$ defined by the piecewise affine interpolation of this discrete high-resolution spectrum on the wavenumber range, and simulate measurements by integrating numerically (1) with the kernel (4) using Romberg's method [12]. Finally, a Gaussian noise with variance $\sigma^2 = 10^{-3}$ is added to the measurements, which produces a realistic measurement vector with dimension $M = 319$ and peak-signal-to-noise ratio around 60 dB. Note that we do not simulate the measurements with the discretized model, which would put us in a situation of inverse crime [13, Section IV.C] and would lead us to erroneous or unjustified conclusions.

We then process these simulated data with the three models considered above (Riemann sum discretization, Fourier basis approximation, Fourier-affine basis approximation), solving the least squares problem by applying the pseudo-inverse of the associated matrix ($\boldsymbol{A}$ or $\boldsymbol{H}$) to the measurement vector. To estimate the reconstruction precision, we compute the discrete mean square error

$$\mathrm{MSE}(\boldsymbol{x}^*, \hat{\boldsymbol{x}}) = \frac{1}{K}\|\hat{\boldsymbol{x}} - \boldsymbol{x}^*\|^2$$

between the ground-truth spectrum $x^*(\sigma)$ sampled on the uniform grid $(\sigma_k)_{0\leq k\leq K-1}$ and the reconstruction. Note that this error estimate is the only one possible for the Riemann sum model, but for the approximations models (Fourier and Fourier-affine) the continuous error

$$\mathrm{MSE}_{\mathrm{c}}(x^*, \hat{x}) = \frac{1}{\Delta_\sigma}\int_{\sigma_{\min}}^{\sigma_{\max}} \left(\hat{x}(\sigma) - x^*(\sigma)\right)^2 d\sigma$$

would be more natural. In practice the two values barely differ, so we stick to the discrete MSE to keep comparable estimates for all models.

B. Case of a vanishing spectrum

We first consider the ECOSTRESS spectrum mentioned above (black/blue curve in Figure 1, left). This spectrum vanishes at the boundaries $\sigma_{\min}$ and $\sigma_{\max}$ of the spectral domain, so the constraint $x(\sigma_{\min}) = x(\sigma_{\max})$ imposed by the Fourier basis model is not an issue, and there is no need to consider the Fourier-affine model.

In Figure 1, we can see that the Fourier basis model systematically performs better than the Riemann sum model (the discrete MSE is significantly smaller for each value of K). The improvement is particularly impressive for the lowest-dimensional case ($K = 65$), since in that case the Riemann sum model fails to reconstruct a decent approximation of the ground truth, while the Fourier basis model yields a reconstructed spectrum barely distinguishable from the ground truth. It is important to notice that the complexity is the same for both algorithms, since it only depends on the size ($M \times K$) of the matrix to be (pseudo-)inverted.

Table I shows the contributions of the approximation error and the noise-induced error (the two terms discussed after Equation (15)) to the continuous error $\mathrm{MSE}_{\mathrm{c}}(x_K^*, \widehat{x})$ in the Fourier basis model, for various values of K. The approximation error $\|x^* - x_K^*\|^2$ is computed using Romberg's method to integrate the squared difference between the continuous piecewise affine ground-truth spectrum and its projection on the Fourier basis. The noise-induced error $\|x_K^* - \widehat{x}\|^2$ is, thanks

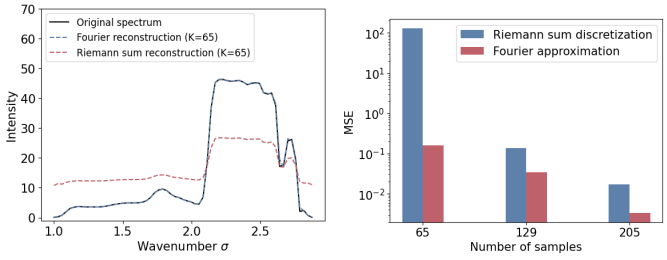

Figure 1: (left) Reconstruction of the spectrum from the measurements using the proposed approach with a Fourier basis and the implicit discretization of the integral operator on a uniform grid for 65 basis functions and 65 samples. Fourier basis functions allow for an accurate reconstruction of the spectrum even for a small number of basis functions. (right) discrete MSE (in log scale) between the ground-truth spectrum and its reconstruction from the measurements using the proposed approach with a Fourier basis and the explicit discretization of the integral operator on a uniform grid. The reconstruction precision is significantly improved using Fourier basis functions to represent the spectrum.

dimension (K)	$\|x^* - x^*_K\|^2$	$\|x^*_K - \hat{x}\|^2$
65	2.15×10^{-1}	8.29×10^{-6}
129	3.5×10^{-2}	4.44×10^{-6}
205	3.8×10^{-3}	3.04×10^{-6}

Table I: Approximation error (squared model bias) and noise-induced error (variance) for various number of Fourier basis functions.

to Shannon-Nyquist Theorem, equal (up to a coefficient $1/K$) to the discrete MSE between the K lowest-frequency Fourier coefficients of the ground-truth spectrum (estimated using Romberg's method) and the corresponding coefficients c_k of the estimated reconstruction. As expected, the approximation error decreases with the number of Fourier basis functions. Moreover, the projection error is very low ($\approx 10^{-6}$) for all values of K, which shows that the least squares reconstruction in the approximation space is nearly optimal in reason of the good signal-to-noise ratio of the simulated measurements.

C. General case (no boundary continuation)

We now consider a non-vanishing spectrum x^*, for which $x^*(\sigma_{\min})$ and $x^*(\sigma_{\max})$ are very different (black/red curve in Figure 2, left). In that case, the Fourier basis model is not very efficient, because of the constraint $x(\sigma_{\min}) = x(\sigma_{\max})$ inherited from the Δ_σ-periodicity of the basis functions. However, the Fourier-affine model proposed in Section IV-B (Fourier basis enriched with an affine component) nicely solves this issue. Indeed, we can see in Figure 2 that the presence of a single additional affine component in the approximation space allows us to get rid of the strong reconstruction artifacts (Gibbs oscillations near the domain boundaries) observed with the Fourier basis model, and improves the reconstruction error by a factor up 1000.

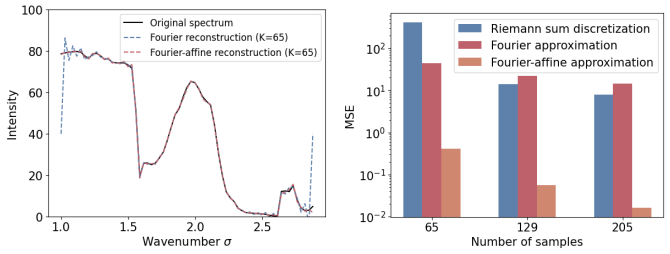

Figure 2: (left) Reconstruction of a non-vanishing spectrum x^* (black plain curve) using a Fourier or a Fourier-affine basis. We can see that Fourier basis reconstruction (blue dashed curve) exhibits strong oscillations near the boundaries of the spectral range. Those are in fact Gibbs artifacts caused by the inability of this Fourier basis to deal with the discontinuity existing in the periodical extension of the signal. Fortunately, these artifacts are completely eliminated in the Fourier-affine model (red dashed curve). (right) discrete MSE between x^* and the reconstructions obtained using the three different models for various values of K. Contrary to what we observed in Figure 1, the Fourier model now performs as poorly as the Riemann sum model (because of Gibbs artifacts), but the Fourier-affine model improves the reconstruction error by at least two orders of magnitude.

VI. Conclusion

In this paper, we proposed a new way to discretize linear integral operators in an inverse problem arising in hyperspectral signal reconstruction from interferometric measurements. We showed that, while keeping the efficiency of a direct least-square inversion and with no additional computational cost, the classical discretization with a Riemann sum can be advantageously reformulated using an approximation space obtained by enriching a Fourier basis with an affine component to avoid Gibbs artifacts. With numerical experiments, we demonstrate on realistic simulated data that the proposed method improves the reconstruction error by one to three orders of magnitude. More generally, we advocate the idea that enriching further the proposed Fourier-affine basis with functions able to better represent some identified classes of spectra (vegetation spectra, soil spectra, mineral spectra) could lead to even more accurate reconstructions.

VII. Acknowledgements

This work was supported by the French National Research Agency (ANR) under the project FuMultiSPOC (ANR-20-ASTR-0006).

References

[1] D. Blumstein *et al.*, "IASI instrument: Technical overview and measured performances," *Proceedings of SPIE - The International Society for Optical Engineering*, vol. 5543, Nov. 2004.

[2] S. Gousset *et al.*, "Nanocarb spaceborne miniaturized ghg sensor: first experimental results," in *International Conference on Space Optics—ICSO 2020*, vol. 11852. SPIE, 2021.

[3] Y. Ferrec *et al.*, "Overview of the NanoCarb GHG sensor project," in *OPTRO 2022, Int. Symp. on Optronics in defence and security*, 2022.

[4] J. M. Bioucas-Dias *et al.*, "Hyperspectral remote sensing data analysis and future challenges," *IEEE Geoscience and remote sensing magazine*, vol. 1, no. 2, 2013.

[5] M. Jouni, D. Picone, and M. Dalla Mura, "Model-based spectral reconstruction of interferometric acquisitions," in *ICASSP 2023*. IEEE, 2023.

[6] P. Escande and P. Weiss, "Sparse wavelet representations of spatially varying blurring operators," *SIAM Journal on Imaging Sciences*, vol. 8, no. 4, 2015.

[7] ——, "Fast Wavelet Decomposition of Linear Operators through Product-Convolution Expansions," Jul. 2020.

[8] W. Dahmen, S. Prößdorf, and R. Schneider, "Wavelet approximation methods for pseudodifferential equations II: Matrix compression and fast solution," *Advances in computational Mathematics*, vol. 1, 1993.

[9] D. Picone, S. Gousset, M. Dalla-Mura, Y. Ferrec, and E. le Coarer, "Interferometer response characterization algorithm for multi-aperture Fabry-Perot imaging spectrometers," *Optics Express*, vol. 31, no. 14, Jul. 2023.

[10] S. Mallat, *A wavelet tour of signal processing: the sparse way*, 3rd ed. Amsterdam Boston: Elsevier/Academic Press, 2009.

[11] S. K. Meerdink, S. J. Hook, D. A. Roberts, and E. A. Abbott, "The ecostress spectral library version 1.0," *Remote Sensing of Environment*, vol. 230, 2019.

[12] W. Romberg, "Vereinfachte numerische integration," *Norske Vid. Selsk. Forh.*, vol. 28, 1955.

[13] M. Guerquin-Kern, L. Lejeune, K. P. Pruessmann, and M. Unser, "Realistic analytical phantoms for parallel magnetic resonance imaging," *IEEE Transactions on Medical Imaging*, vol. 31, no. 3, 2011.